Computational Materials Science 51 (2012) 117–121

Contents lists available at ScienceDirect

Computational Materials Science

journal homepage: www.elsevier.com/locate/commatsci

Rate dependent deformation of a silicon nanowire under uniaxial compression: Yielding, buckling and constitutive description

Chi Yan Tang [a], L.C. Zhang [b,*], Kausala Mylvaganam [b]

[a] School of Aerospace, Mechanical and Mechatronic Engineering, The University of Sydney, NSW 2006, Australia
[b] School of Mechanical and Manufacturing Engineering, The University of New South Wales, NSW 2052, Australia

ARTICLE INFO

Article history:
Received 14 June 2011
Accepted 21 July 2011

Keywords:
Si nanowire
Strain rate
Buckling
Molecular dynamics

ABSTRACT

This paper investigates the effect of compressive strain rate on the mechanical behaviour of single crystalline silicon nanowires using molecular dynamics simulation. It was found that of the whole range of the strain rates studied, the initial deformation of a nanowire is elastic. At lower strain rates the nanowire exhibits greater elasticity, and simple constitutive equations can be developed to describe the nanoscale structure and its deformation mechanism. With the increase in strain rate, the buckling stress increases and becomes steady at medium strain rates. On applying a very high strain rate, which is equivalent to a mechanical shock, the maximum buckling stress has a sudden rise and the silicon nanowire undergoes ballistic annihilation at both ends.

Crown Copyright © 2011 Published by Elsevier B.V. All rights reserved.

1. Introduction

Silicon nanowires (SiNWs) are key building blocks in nano-electro-mechanical applications and have been used in a wide variety of devices [1–4], such as field effect transistors (FETs), *p–n* diodes, bipolar junction transistors and complementary inverters.

A detailed understanding of the mechanical behaviour of nano-components is largely impeded by the difficulty in accounting for the scale and surface effects in conventional continuum mechanics models [5–9]. It is well known in classical mechanics of materials that the strain rate plays an important role in the dynamic plastic behaviour of structures under simple dynamic loads [10,11]. For example, mild steel with varying ferrite grain sizes under uniaxial compressive tests [12] has a significant increase in the upper yield stress with increasing the strain rate. Other materials such as titanium and aluminium 60116-T6 are shown to be less sensitive [13]. Theoretically, the strain-rate sensitivity of idealized elastic–plastic linear hardening material under the impact of a mass [14] has also been studied with the aid of the Cowper–Symonds equation [15].

The effect of strain rate on the behaviour of nano-mechanical components has not been deeply understood due to the difficulties in experimentation. An early molecular dynamics study [16] of Ni nanowires under uniaxial strain using an embedded-atom (many-bodied) potential reported that for strain rates from 0.05% to 15% ps^{-1}, the nanowire behaved elastically up to the strain of 11.5% at the stress of 9.4 GPa. The Ni nanowire had a higher fracture point with different strain rates. At low strain rates, it deformed plastically although its structure remained crystalline. Necking was observed before fracture. At high strain rates, the structure changed from a crystalline to amorphous without necking and the material flowed like a liquid. In a more recent study, Wen et al. [8] applied the tensile strain according to $\Delta\varepsilon_z = \dot{\varepsilon}\Delta t$, where $\dot{\varepsilon}$ is the strain rate and Δt is the time step and reported that two critical strain rates played pivotal role in switching between plastic deformation modes. Ikeda et al. [17] found that under high strain rates, single crystal Ni and NiCu random alloy nanowires in tension exhibit transformations from crystalline to amorphous phase, and that the nanowires experience dramatic changes in the atomic short-range order as well as a near vanishing of the tetragonal shear elastic constant perpendicular to the tensile direction. A Ni nanowire showed a much higher yield stress of 5.5 GPa in comparison with that of its bulk form. In a study on a copper nanowire, Wu et al. [18] showed that strain rate had an influence on the strength of the nanowire. At a low strain rate, its deformation was with dislocations and twins, while at a high strain rate amorphisation became a dominant factor. Using molecular dynamics, Guo et al. [19] reported that the yield stress of single-crystal copper blocks under simple shear was insensitive to the strain rate below a critical strain rate. For FCC metals, Koh and Lee [20] found that Pt and Au nanowires under different strain rates (4.0×10^8, 4.0×10^9 and 4.0×10^{10} s^{-1}) had distinct deformation modes, crystalline-ordered, mixed-mode and amorphous-disordered deformation modes. Jing et al. [21] investigated the effect of temperature, length and strain rate on the buckling behaviour of silicon nanowire. As the applied strain rates varied from 0.01% ps^{-1} to 0.1%

* Corresponding author. Address: Mechanical Engineering Building (J17), School of Mechanical and Manufacturing Engineering, The University of New South Wales, NSW 2052, Australia. Tel.: +61 2 9385 6078; fax: +61 2 9385 7316.
E-mail address: Liangchi.Zhang@unsw.edu.au (L.C. Zhang).

0927-0256/$ - see front matter Crown Copyright © 2011 Published by Elsevier B.V. All rights reserved.
doi:10.1016/j.commatsci.2011.07.037

ps^{-1} the buckling load increased linearly. From the load–strain curves they found that the elastic properties of a nanowire are insensitive to strain rate.

The present work will explore the mechanical shock induced deformation of a SiNW in nano-electromechanical components, including the variation of the buckling stress with the strain rates.

2. Modelling and computational details

The SiNW model (Fig. 1) used in this study consists of crystalline silicon atoms with a length of 32.79 nm. The cross-section of the SiNW is hexagonal in the (1 1 0) plane with an average radius of 1.17 nm. This cross-section was chosen due to its structural stability [22]. To investigate the end-effects during dynamic loading, two scenarios were studied: (i) a hexagonal-profiled nanowire with fixed atoms along both ends, and (ii) the same nanowire but with additional silicon atoms which form an atomic wall at both ends of the nanowire. Both silicon nano-wires consist of 8855 free-moving Newtonian silicon atoms while the ends of the nanowires were held rigidly. The two fixed ends were pushed inwards along the axial direction in small steps in order to simulate uni-axial compression. The applied strain rates vary in magnitude from 1.52×10^8 to $9.6 \times 10^9\ s^{-1}$ across different simulation runs. The SiNW models had been shown to be sufficiently large and long in order to minimize the effects of the boundaries and to satisfactorily simulate uni-axial compression. As the directionality of silicon bonding is important, the three-bodied Tersoff potential was used in the molecular dynamic simulations [23,24]. The silicon atoms were assumed to be chemically inert and that the deformation of the SiNW take place in a vacuum environment. It had been demonstrated in many studies that the Tersoff potential can adequately predict stable crystalline and amorphous phases [7,25–34].

The simulations were performed at 293 K with a time-step of 2.5 fs on a SGI Altix 3700 Bx2 cluster *via* high-performance OpenMP parallel computation in a shared-memory architecture.

The steepest descent method was used to iteratively minimize the total energy of the system so that the structure of a silicon nano-wire is energetically optimized prior to compressive loading. The energy against iterative time step is shown in Fig. 2. The point of minimum energy in this curve represents the most stable configuration of silicon atoms of the nanowire. The energy has almost converged after a total of 74 and 88 iteration steps for the nanowires without and with walls, respectively. The inner silicon atoms of the nano-wire show negligible change in position; however the radius of the SiNW drops by 0.46% (no wall) and 0.41% (with wall) as a result of the shrinkage of energetically unfavourable lesser-coordinated outer layer atoms. A related study on the annealing and relaxation of a SiNW over a thousand time-steps showed

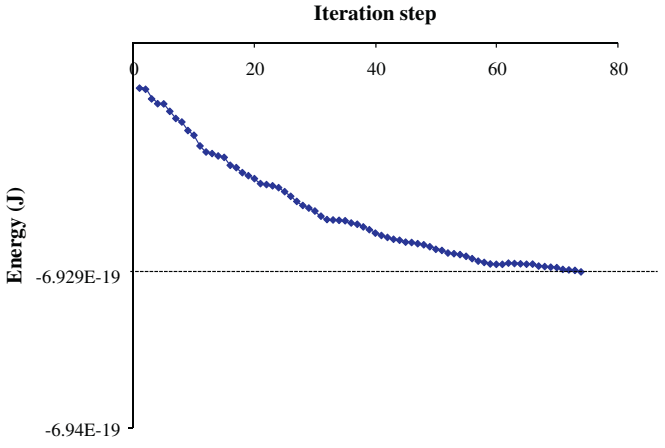

Fig. 2. Energy against iteration step for the Si-NW without a wall.

similar results [7]. The expansion along the axial direction has been shown to be negligible.

3. Results and discussion

3.1. Strain rate effect on the stress–strain behaviour

Fig. 3 shows the engineering stress–strain relationship of the SiNW under compression for three different strain rates. The stresses are derived by averaging the instantaneous sums of the total atomic forces at the two ends over 100 consecutive time-steps. This would eliminate statistical noise that arises from the fluctuations in forces.

For all different strain rates, the initial elastic deformation regime is characterized by linear stress–strain behaviour in both with and without wall simulations. At smaller strain rates, the stress–strain curves exhibit greater linearity, indicating that the nanowires exhibit greater elasticity. The peak of the stress–strain curve is the primary signal in determining the onset of dynamic buckling while the fall after the peak characterizes the post-buckling deformation with strain-rate induced amorphisation. It is clear that larger strain rates increase the level of the buckling load. This is consistent with a previous study conducted on nanocrystalline copper, which found that lowering the strain rate by an order of magnitude would almost remove the overshoot in the stress–strain curves [35]. This phenomenon was also seen in a study related to the strain-rate induced amorphisation of metallic nanowires [17]. Virtually identical results are obtained from repeated simulations for both the SiNW models defined above.

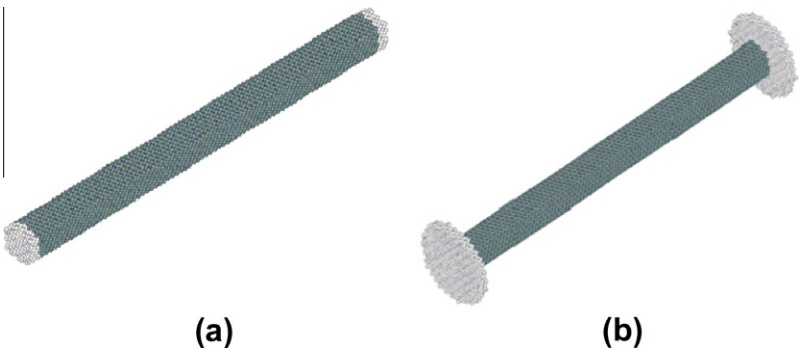

Fig. 1. (a) Three-dimensional view of the initial silicon nano-wire model. (b) The model includes an atomic "wall" at both ends of the nanowire. The cross-section of the SiNW is in the (1 1 0) plane. The clear spheres represent fixed atoms.

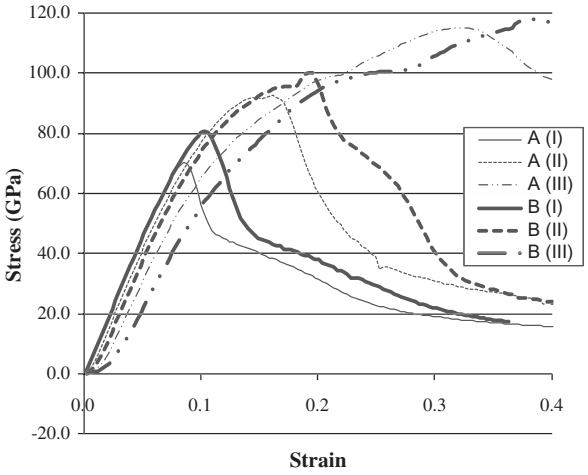

Fig. 3. Stress–strain relationship of SiNWs under compression. Different strain rates have an effect on the curve and critically effects on the onset of buckling. The legends A, B correspond to the simulations without and with the wall, respectively. The legends (I), (II), (III) correspond to the strain rates 1.52×10^8 s^{-1}, 6.1×10^8 s^{-1} and 1.63×10^9 s^{-1}, respectively.

3.2. Strain rate effect on buckling

The differences between the nanowires with and without the wall are that the former contains a slightly larger cross-sectional area at the edges due to the surrounding wall atoms. Fig. 4 shows the effect of the strain rate on the critical buckling stress. The buckling stress is 69.1–116.7 GPa under lower strain rates (1.5×10^8 s^{-1}–1.0×10^9 s^{-1}), and remains steady under medium strain rates (1.0×10^9 s^{-1}–1.9×10^9 s^{-1}). The simulations with walls typically exhibit a higher buckling stress at small strain rates compared to the case without the wall. It was found that the critical buckling stress ($\sigma_{buckling}$) at the lower strain rates can be approximately described by,

$$\log(\sigma_{buckling}) = k_0 \log(\dot{\varepsilon}) + k_1 \tag{1}$$

where k_0, and k_1 are constants while $\dot{\varepsilon}$ represents the strain rate. Note that for strain rates less than 6.0×10^8 s^{-1}, the buckling stresses are relatively constant but they increase rapidly for higher strain rates. The initial increase in the onset of buckling is analogous to static and dynamic buckling of columns in continuum mechanics.

At higher strain rates (>1.9×10^9 s^{-1}), the maximum buckling stress exhibits a sudden jump. On analysing the structure, we found that this is due to the ballistic annihilation where the fixed

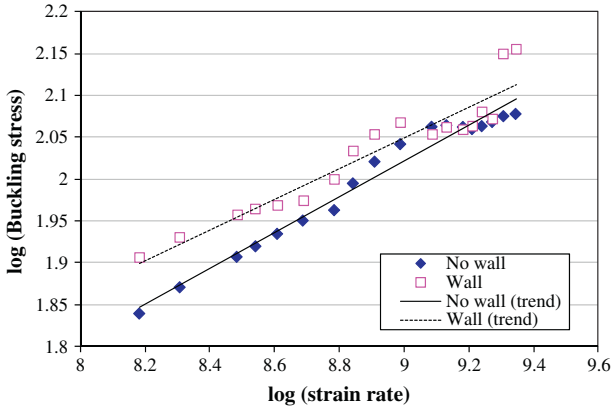

Fig. 4. The effect of strain rate (s^{-1}) on the buckling stress (GPa), filled diamonds represent simulations without a wall and the squares represent simulations with a wall, respectively.

silicon atoms of both ends penetrate into the nanowire. Fig. 5 displays a nanowire undergoing ballistic annihilation. Note that both ends of the atoms grow to a clump of amorphous atoms while the centre of the nanowire remains structurally intact due to the lack of the propagation of the induced stresses. A comparison with the predicted buckling stress in conventional continuum mechanics would yield useful insights into the scale and surface effects that occur. The predicted critical buckling force (Euler buckling) for a column with both ends built-in is given [10] by,

$$P = \frac{4\pi^2 EI}{L^2} \tag{2}$$

where E is the modulus of elasticity and I is the second moment of area (also known as second moment of inertia) along the neutral axis. In our calculations, E was estimated by averaging the slopes of the stress–strain curves across different strain rates and was found to be 625.6 GPa; I was estimated to be 16,809.2 Å^4 by approximating the cross-section as a filled hexagonal profile. The simulated critical buckling force at low strain is 69.11 GPa while the predicted critical buckling force according to Eq. (2) is 47.77 GPa. These values vary by a factor of 1.45. This discrepancy is attributed to the effect of a comparatively large surface area and the scale effect that arises from the dominant surface–surface interactions.

Fig. 6 displays the effect of the strain rate on the buckling strain; the relationship between these two parameters is similar to the relation between buckling stress and strain rate, and can be expressed as:

$$\log \varepsilon_{buckling} = \alpha_0 \log(\dot{\varepsilon}) + \alpha_1 \tag{3}$$

which is similar to the stress law, where α_0, α_1 are constants and calculated via the least-squares regression. The regression analysis is made over the entire range of strain rates studied. For the SiNW with no wall, the calculated α_0 and α_1 values are 0.6125 and −6.1449, respectively, and for the SiNW with wall, they are 0.5686 and −5.6666, respectively. The R-square statistics is calculated to be 0.98 and 0.97 for the cases without and with wall, respectively. This indicates a linear satisfactory fit between the logarithms of the buckling strain and the strain rate. Under lower strain rates, the onset of buckling experiences a gradual linear increase, but under higher strain rates the increase is rapid due to the dynamic buckling and ballistic annihilation. This indicates that the increase of the critical stress and strain levels due to a higher strain can be viewed as an overshoot of the elastic region.

Fig. 7 shows the relationship between the buckling strain and buckling stress, which can be expressed using the following formula:

$$\log(\sigma_{buckling}) = \beta_0 \log(\varepsilon_{buckling}) + \beta_1 \tag{4}$$

where β_0 and β_1 are constants. For the SiNW with the wall, *via* a least-squares regression, β_0 and β_1 are found to be 0.3411 and 2.2363, respectively. The regression analysis was made over the entire range of strain rate values in this study. For the SiNW without the wall, β_0 and β_1 are 0.3163 and 2.2226, respectively. The R-square statistics are 0.95 and 0.90 for the cases without and with the wall, respectively. This indicates a linear satisfactory fit between the logarithms of the buckling stress and the buckling strain.

Thus, in compression, the strain rate plays a critical role in determining the onset of buckling. For the two cases considered, the different critical buckling strain and stress levels at high strain rates can be characterized as an overshoot of the elastic region. At ultra high strain rates, the conventional buckling mechanisms are substituted with ballistic annihilation.

Fig. 8 displays the number of the higher-coordinated amorphous atoms for both models at different strain rates and this information can be used to determine the point in which the defor-

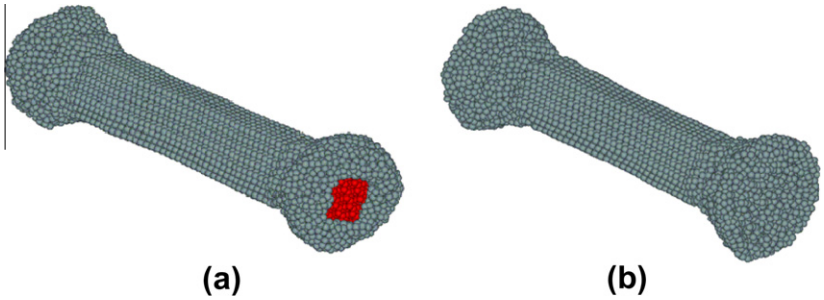

Fig. 5. Silicon nanowire undergoing ballistic annihilation under ultra-high strain. (a) and (b) indicate the SiNW without and with a wall, respectively. The atoms indicated in red are fixed atoms.

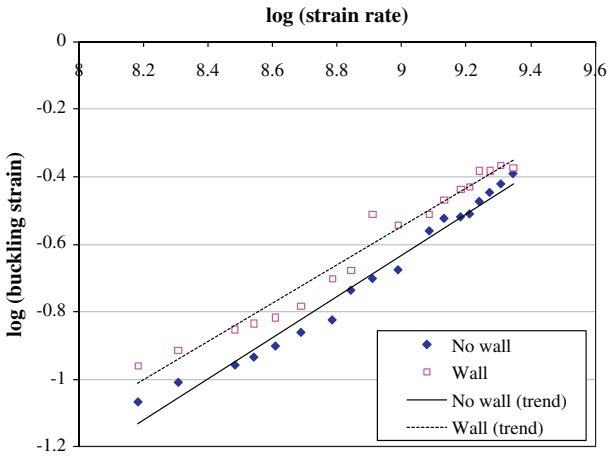

Fig. 6. The effect of strain rate (s^{-1}) on the buckling strain. The filled diamonds and unfilled squares represent simulations without and with the wall, respectively.

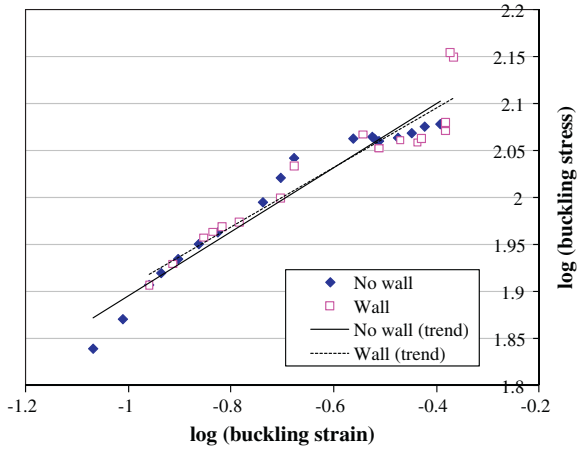

Fig. 7. The relationship between buckling stress (GPa) and buckling strain.

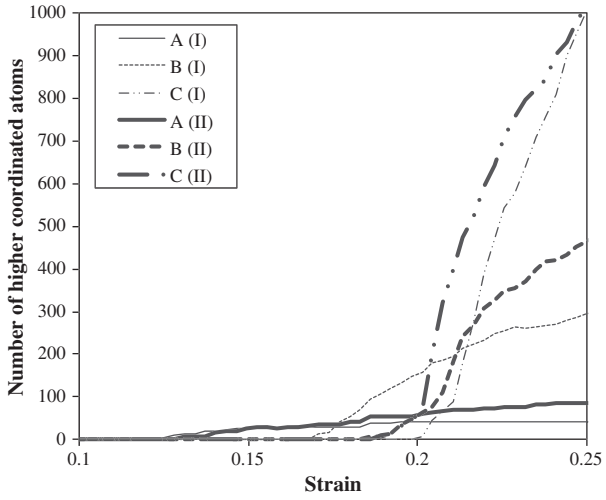

Fig. 8. Number of higher coordinated amorphous atoms against strain for the two SiNW models. The legends A, B and C correspond to the strain rates $1.52 \times 10^8\ s^{-1}$, $6.1 \times 10^8\ s^{-1}$ and $1.63 \times 10^9\ s^{-1}$ respectively. (I) and (II) indicate simulations without and with the wall, respectively.

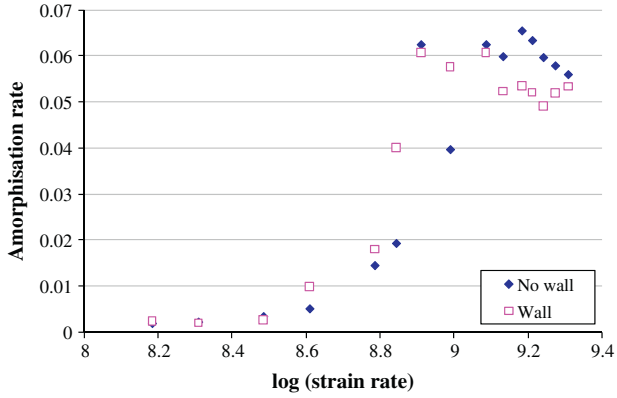

Fig. 9. Amorphisation rate (number of amorphous atoms growth per timestep) over log (strain rate) (s^{-1}).

mation of the SiNW becomes irreversible. It can be seen that there are more higher-coordinated atoms in the SiNW with a wall at higher strains ($\varepsilon > 0.22$).

Fig. 9 displays the amorphisation rate against strain rate. The amorphisation rate is obtained by calculating the increase of amorphous atoms in 10,000 timesteps preceding the point in which amorphisation starts taking place. The amorphisation rate increases with greater strain rates until a critical value. For strain rates above this critical value, the deformation mode is characterized by superplasticity at both ends. At an ultra high strain ($\dot{\varepsilon} = 4.88 \times 10^9\ s^{-1}$), the fixed atoms penetrate into the free-moving Newtonian silicon atoms as displayed in Fig. 5.

3.3. Applicability of constitutive equations

For a strain-rate-sensitive material such as SiNWs, the yield stresses will show dependence on strain rate via a modified Cowper–Symonds constitutive equation [10,14,19, 36] given by:

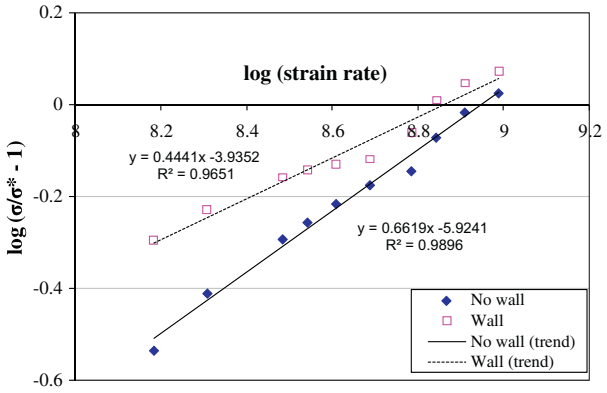

Fig. 10. Relationship between $\lg\left(\frac{\sigma}{\sigma^*}-1\right)$ and $\lg\dot{\varepsilon}$. The filled diamonds and unfilled squares represent simulations without and with the wall, respectively.

$$\sigma = \sigma^*\left[1 + c\left(\frac{\dot{\varepsilon}}{\dot{\varepsilon}_c}\right)^p\right] \tag{5}$$

where σ is the rate-dependent yield stress, $\dot{\varepsilon}$ is the applied strain rate, σ^* is the quasi-static yield stress and $\dot{\varepsilon}_c$ represents the critical strain rate, where lower applied strain rates do not exhibit strain-rate dependent behaviour. The exponent p represents the strain rate sensitivity.

The above equation can be rewritten as:

$$\lg\left(\frac{\sigma}{\sigma^*}-1\right) = p\lg\dot{\varepsilon} + (\lg c - p\lg\dot{\varepsilon}_c) \tag{6}$$

The yield stresses are obtained by determining the stress level in which the initial crystalline structure of the SiNW starts disintegrating into amorphous bonds. At this point, the SiNW deformation becomes irreversible when reversing the direction of the applied load at both ends, i.e., it becomes no longer possible for the initial crystalline structure to be recovered. The determination of the yield stress from the stress–strain curve alone is impeded with ambiguity, as these structures do not fully recover elastically when reversing the direction of the applied load on a deformed SiNW. The quasi-static values are approximated by applying a very small strain at small strain rates along both ends.

Fig. 10 displays $\lg\left(\frac{\sigma}{\sigma^*}-1\right)$ as a function of $\lg(\dot{\varepsilon})$ for both the SiNW models. The value $c = 0.1$ is chosen so that the critical strain rate is defined as the strain rate where the yield stress is higher than the quasi static value by a factor of 1.1 [20].

At smaller strain rates, the Cowper–Symonds equation is valid due to a linear relationship between $\lg\left(\frac{\sigma}{\sigma^*}-1\right)$ and $\lg(\dot{\varepsilon})$. The values of p are found to be, via least-squares fitting, 0.6619 and 0.4441 for the SiNWs without and with a wall, respectively. The critical strain rate $\dot{\varepsilon}_c$ is deduced from the intercept of this curve fit and has a value of $2.75 \times 10^7\ s^{-1}$ and $4.44 \times 10^6\ s^{-1}$, respectively. These values indicate that under a low strain rate the behaviour of a SiNW is not dependent on strain-rate. Under larger strain rates, the Cowper–Symonds equation is no longer valid as the structure is dominated by ballistic annihilation that arises from the inability of the structure to propagate the stress waves. This phenomenon is observed in both the nanowires with and without the wall.

4. Conclusion

With the aid of the molecular dynamics analysis, this study has acquired the effect of compressive strain rate on the mechanical behaviour of silicon nanowire. The study draws the following conclusions:

(i) Under low strain rates, the nanowire exhibits greater elasticity.
(ii) With the increase in strain rate, the onset of buckling stress increases and becomes steady when the strain rate reached a certain value. In this range, the Cowper–Symonds equation can be used to describe the SiNW response to dynamics compression. The deformation of the SiNW exhibits a very strong dependence on the strain rate.
(iii) Under very high strain rates, the SiNW structure undergoes ballistic annihilation at both ends, and the Cowper–Symonds equation is no longer applicable.

Acknowledgements

The authors acknowledge the National Computational Infrastructure (NCI) for support and provision of supercomputing facilities. The continuous financial support from the Australian Research Council (ARC) is very much appreciated.

References

[1] D. Appell, Nature 419 (2002) 553–555.
[2] S.W. Chung, J.Y. Yu, J.R. Heath, Applied Physics Letters 76 (2009) 2068–2070.
[3] Y. Cui, Q. Wei, H. Park, C.M. Lieber, Science 293 (2001) 1289–1292.
[4] Y. Huang, X. Duan, Y. Cui, L.J. Lauhon, K.H. Kim, C.M. Lieber, Science 294 (2001) 313–317.
[5] M. Menon, D. Srivastava, I. Ponomareva, L.A. Chernozatonskii, Physical Review B 70 (2004). 125313/1–6.
[6] R.E. Miller, V.B. Shenoy, Nanotechnology 11 (2000) 139–147.
[7] C.S. Moura, L. Amaral, Nuclear Instruments and Methods in Physics Research B: Beams Interactions with Materials and Atoms 228 (2005) 37–40.
[8] Y.H. Wen, Z.Z. Zhu, R.Z. Zhu, Computational Materials Science 41 (2008) 553–560.
[9] H.A. Wu, AK. Soh, International Journal of Nonlinear Sciences and Numerical Simulation 4 (2003) 233–238.
[10] N. Jones, Structural Impact, Cambridge University Press, 1989.
[11] T. Nicholas, Material behavior at high strain rates, in: J.A. Zukas, T. Nicholas, H.F. Swift, L.B. Greszczuk, D.R. Curran (Eds.), Impact Dynamics, John Wiley, New York, 1982, pp. 277–332.
[12] K.J. Marsh, J.D. Campbell, Journal of the Mechanics and Physics of Solids 11 (1963) 49–63.
[13] C.J. Maiden, S.J. Green, Journal of Applied Mechanics 33 (1966) 496–504.
[14] D. Karagiozova, N. Jones, Journal of Applied Mechanics 64 (1997) 93–200.
[15] G.R. Cowper, P.S. Symonds, Technical Report, vol. 28, Brown University, 1957.
[16] P.S. Branicio, J.P. Rino, Physical Review 62 (2000) 16950–16955.
[17] H. Ikeda, Y. Qi, T. Çagin, K. Samwer, W.L. Johnson, W.A. Goddard III, Physical Review Letters 82 (1999) 2900–2903.
[18] H.A. Wu, A.K. Soh, X.X. Wang, Z.H. Sun, Key Engineering Materials 261–3 (2004) 33–38.
[19] Y. Guo, Z. Zhuang, X.Y. Li, Z. Chen, International Journal of Solids and Structures 44 (2007) 1180–1195.
[20] S.J.A. Koh, H.P. Lee, Nanotechnology 17 (2006) 3451–3467.
[21] Y. Jing, Q. Meng, Y. Gao, Computational Materials Science 45 (2009) 321–326.
[22] K. Mylvaganam, L.C. Zhang, Journal of Computational and Theoretical Nanoscience 2 (2005) 385–388.
[23] J. Tersoff, Physical Review B 39 (1989) 5566–5568.
[24] J. Tersoff, Physical Review Letters 56 (1986) 632–635.
[25] D.A. Broido, A. Ward, N. Mingo, Physical Review B 72 (2005). 014308/1–8.
[26] W.C.D. Cheong, L.C. Zhang, H. Tanaka, Key Engineering Materials 196 (2001) 31–42.
[27] W.C.D. Cheong, L.C. Zhang, Key Engineering Materials 233–236 (2003) 603–608.
[28] K. Mylvaganam, L.C. Zhang, Nanotechnology 13 (2002) 623–626.
[29] J.W. Kang, H.J. Hwang, Nanotechnology 14 (2003) 402–408.
[30] C.Y. Tang, L.C. Zhang, Nanotechnology 16 (2005) 15–20.
[31] Z. Tang, Y. Xu, G. Li, N.R. Aluru, Journal of Applied Physics 114304 (2005) 1–13.
[32] I. Zarudi, W.C.D. Cheong, J. Zou, L.C. Zhang, Nanotechnology 15 (2004) 104–107.
[33] L.C. Zhang, H. Tanaka, Tribology International 31 (1998) 425–433.
[34] L.C. Zhang, H. Tanaka, JSME International Journal, Series A: Solid Mechanics & Material Engineering 42 (1999) 546–559.
[35] J. Schiøtz, K.W. Jacobsen, Science 301 (2003) 1357–1359.